PSFC/JA-02-5

Investigation of the Origin of Neutrals in the Main Chamber of Alcator C-Mod

B. Lipschultz, B. LaBombard, C.S. Pitcher, R. Boivin[1]

March 2002

Plasma Science and Fusion Center
Massachusetts Institute of Technology
Cambridge, MA 02139 USA

[1]Currently at General Atomics, La Jolla, CA 92186 USA

This work was supported by the U.S. Department of Energy, Cooperative Grant No. DE-FC02-99ER54512. Reproduction, translation, publication, use and disposal, in whole or in part, by or for the United States government is permitted.

Submitted for publication to *Plasma Physics and Controlled Fusion.*

Investigation of the origin of neutrals in the main chamber of Alcator C-Mod

B. Lipschultz, B. LaBombard, C.S. Pitcher and R. Boivin‡
Massachusetts Institute of Technology Plasma Science & Fusion Center Cambridge Ma. 02139 U.S.A.
‡currenly at General Atomics, La Jolla Ca. 92186 U.S.A.

Abstract: A series of experiments are described which are aimed at quantifying the relative contribution of divertor leakage and radial ion transport on neutral pressures surrounding the core plasma. Evidence is presented implying that cross-field transport competes with, or dominates, parallel transport in such a way that plasma exists far out in the Scrape-Off Layer (SOL) in the shadow of limiters and recycles on main chamber surfaces. The transition from L- to H-mode core confinement does not affect the far SOL characteristics nor the scaling of pressures around the plasma.

Variations in magnetic equilibrium are used to vary the divertor pressures independent of the core plasma. Based on the analysis of such experiments using a simple neutral flow model we estimate that neutrals escaping from leaks in the lower (closed) divertor during lower x-point operation contribute a smaller fraction (~10-30%) of the midplane pressure than main chamber recycling. The inferred leakage is much larger from the upper (open) divertor during upper x-point operation. Most neutrals escaping from either divertor do not directly travel to the midplane. Instead, they are redirected, most likely by some combination of ionization and/or collisions (elastic, charge exchange).

*E-mail address: Blip@psfc.mit.edu

1. Introduction

The Scrape-Off Layer (SOL) affects a number of aspects of tokamak operation. Plasma conditions outside the plasma core determine the characteristics of the divertor plasma and therefore the parallel power and particle flow profile at divertor or limiter surfaces. The resultant divertor impurity sources and helium compression in the divertor are also important. Moreover, the SOL can be very important for directly affecting the core - impurity sources in the main chamber, boundary conditions of density and temperature, and in particular, fueling and particle control.

There are two routes for neutrals to arrive in the region outside the core plasma, from which they may reach the core: 1) through radial ion transport to the main chamber surfaces with resultant recycling and creation of neutrals; and 2) by neutral leakage from the divertor (for a diverted plasma). In this paper we describe a series of experiments aimed at assessing the relative roles of these two paths for affecting the main chamber neutral pressure. These include variations in geometry, magnetic equilibrium, divertor bypass leakage and confinement mode.

Previous experiments concentrating on this subject have shown that cross-field ion transport in Alcator C-Mod [1-5] can lead to large ion fluxes to main chamber surfaces and are of sufficient magnitude to explain main chamber neutral pressures. Strong cross-field transport was also required to explain SOL profiles in ASDEX Upgrade [6].

It is reasonable to expect that the divertor geometry should play a role in neutral control [7,8]. Neutrals could leak from the divertor and directly travel to the midplane. The experimental results on this subject are varied, to say the least. Results from JET [9], JFT-2M [10], and DIII-D [11] indicate that increased divertor closure (geometry as well as closing leaks through the divertor structure) leads to a reduction in the midplane pressure. Results from the closing of leaks on C-Mod and ASDEX Upgrade [12-14], as well as the most recent changes in the JET divertor [15,8],lead to an increase in divertor pressure with no change in midplane pressure . C-Mod experiments utilizing divertor bypass valves also implied little effect on the midplane pressure [7,16].

The variety of experimental results and potential contributors to the midplane pressure call into question whether the axisymmetic poloidal divertor concept is fully understood. It is clear that a better understanding of the limits of the divertor configuration will allow us to make a more quantitative judgement between alternative particle and heat flux handling geometries.

The experiments reported here are aimed at better quantifying the relative contribution of divertor leakage and radial ion transport on the midplane pressure. We add further evidence to already published papers showing that radial particle transport is strong and the accompanying recycling on main chamber surfaces can explain measured neutral pressures. Changing the core

transport from L- to H-mode leads to little or no effect on the far SOL indicating that the flux to the walls has not changed, just the gradients at the separatrix and the density in the core..

In an effort to assess the divertor leakage contribution to the midplane pressure we varied upper and lower divertor pressures (and by inference divertor leakage) independent of core density. Based on a simple model we are able to estimate that neutral leakage from the lower divertor during lower single-null discharges contributes between ~10-30% of the midplane pressure, the rest supplied by main chamber recycling. The contribution to the midplane pressure due to leakage out of the upper divertor during upper single-null discharges is of similar magnitude as the contribution from main chamber recycling.

2. Experimental description

All results reported in this paper were obtained with deuterium discharges with $B \times \nabla B$ towards the bottom of the vessel. For most discharges the x-point was located at the bottom of the vessel where the closed, vertical plate divertor, is located (Fig. 1a). Unless otherwise specified all discharges are in L-mode and utilize D_2 as the fill gas. Some experiments required the dominant x-point to be located at the top of the vessel where the divertor is completely open (Fig. 1a).

Alcator C-Mod, like most tokamaks, lacks toroidal (and poloidal) symmetry of the main chamber surfaces outside the divertor. Fig. 1b illustrates this. There are three poloidal limiters and four ICRF antennas (with the accompanying 4 side limiters shown) located at different points toroidally. Even the open upper divertor has 20 thin (1.25 cm toroidally) plates located near ports used to strengthen the vessel. These are shown in profile in Fig. 1a as a dotted line. Each plate has protection tiles on the edges facing the plasma.

The general characteristics and diagnostics of the Alcator C-Mod device can be found elsewhere. Further details on some of the edge diagnostics have also been published previously [12,4]. Here we present some of the more relevant diagnostic descriptions.

The locations of the various pressure diagnostics are shown in Figures 1a-b. Baratron capacitance manometer gauges (~50 ms response time) are located in vertical ports connected to the upper and lower divertors as well as at the midplane of the torus in a large horizontal port. There are two such gauges in the lower divertor, one of which is located at a port (herein called an ‘open’ port) which has a large opening in the outer divertor plate over the port (for diagnostic penetration) through which neutrals can escape back to the main chamber. The second Baratron gauge is located at a port without a diagnostic opening (‘closed’ port where neutral leakage is minimal). Other gauges include a shielded Bayard-Alpert ionization gauge (response time ~ 30 ms), located at the outer midplane, and several Penning gauges (response time < 5 ms), located at several points toroidally (see Fig. 1b) and poloidally (Fig. 1a). All gauges are calibrated against

the Baratron gauges. The Penning gauges have the additional constraint of requiring the full toroidal magnetic field on at the time of calibration. It is important to point out that the only diagnostic we have of the upper divertor is the Baratron gauge mentioned above.

The outer divertor bypass system [16] allows the neutral leakage through the closed lower divertor to the main chamber to be varied dynamically during a discharge. There are 10 discrete toroidally–spaced valves, the locations of which are shown in Fig. 1b.

High resolution profiles of electron temperature and density in the SOL are obtained from two scanning probe systems, both of which are shown in Fig. 1a: a vertical-scanning probe that samples plasma at a position 'upstream' from the entrance to the outer divertor, and a horizontally-scanning probe that records plasma conditions 10 cm above the midplane.

For the experiments described herein we vary the magnetic equilibrium from lower to upper x-point. The measure of the equilibrium variation is the radial gap between the first and second separatrix mapped to the outer midplane, denoted by the parameter SSEP in the EFIT equilibrium solver code [17]. SSEP is negative for lower x-point dominant, positive for the upper null. Typical minimum values are -15 to -20 mm for lower x-point equilibria, but often the magnitude of SSEP is larger.

3. Main chamber sources of neutrals due to cross-field ion flow

In the introduction we referred to two potential contributors to the neutral population surrounding the plasma (in general we are referring to the neutral density at the outer midplane): 1) ion fluxes recycling off main chamber surfaces as neutrals; and 2) neutral leakage from the divertor. Note that the former forms a circuit of ions transported across the magnetic field, flowing out of the core and SOL, and returning to the core and SOL as neutrals. The latter forms a different circuit – ions leave the SOL by flowing along the field into the divertor, recycling as neutrals and reentering the core or SOL (leaking through divertor structure) where they are ionized, closing the loop. In this section we will first discuss the evidence for the existence and magnitude of the first loop.

3.1 General characterization

We briefly review the characteristics of the SOL and the techniques used in this section. Figure 2 includes density (Fig. 2a) and temperature (Fig. 2b) profiles across the SOL for 9 different core densities $1\text{x}10^{20}$ m^{-3} $\leq \bar{n}_e \leq 2.6\text{x}10^{20}$ m^{-3} ($0.17 \leq n_{Greenwald} \leq 0.45$), derived from the horizontal scanning probe. The distance from the separatrix is labeled ‘ρ’. The location of the limiter is indicated, varying from ρ =19-22 mm for these data. The near SOL (ρ ≤ 4.0 mm) has a short e-folding length that is similar to its width. The density at the limiter and in its

shadow is strongly dependent on $\bar{n}_e$. At the two highest densities shown the density profile near the separatrix flattens as well.

Such a characterization of the density profile in the SOL as two regions has been recorded on most divertor tokamaks. See, for example, References [18,19,6,20,12] The differences in gradients between the near and far SOL have been modeled as due to differences in radial ion transport [21,6,22,1,2,4] with cross field diffusion in the far SOL exceeding Bohm values. We note also that density profiles with such 'shoulders' have also been explained as due to non-local neutral sources [18,23].

The temperature near the separatrix varies little as one might expect from a region where parallel conduction dominates energy transport. The temperature gradients near the separatrix vary little as $\bar{n}_e$ is increased. The gradient scale length gradually increases as a function of ρ. In the region beyond the limiter, the temperature is almost always in the range 5-10 eV with little gradient. There are examples of a high temperatures in the far SOL from other tokamaks going back many years [24,25].

As the density is increased beyond the range shown here, the flat region of the density profile starts moving inside the separatrix . At the same time the separatrix temperature drops, indicative that parallel conduction is no longer determining the temperature there. The details of the evolution of SOL conditions as the density limit is approached can be found elsewhere [5].

In previous work [4] we have developed an interpretive analysis of probe profiles to determine radial ion fluxes, $\Gamma_{\perp,i}$ at the limiter radius. The cross-field ion flux density entering the region between two poloidal limiters, $\Gamma_{\perp,\mathrm{lim}}$ can be determined by integrating the parallel ion current incident on those limiters.

$$\int_{\text{lim./SOL interface}} \Gamma_{\perp,i} \cdot dA_{\perp} \approx - \int_{\text{lim. sides}} \Gamma_{\parallel,i} \cdot dA_{\parallel} \tag{1}$$

The assumption underlying the use of this continuity equation is that ionization in the limiter shadow must be small compared to parallel flux term in the continuity equation. Note that perpendicular transport dominates over parallel transport in the limiter shadow due to the short parallel distance between limiters (0.8 m). Based on the above Eq. 1 becomes:

$$2nc_s / L >> S_i \tag{2}$$

Where L is the toroidal spacing, S_i is the ionization rate density, and c_s is the ion sound speed. For the region between two limiters where the horizontal scanning probe is inserted this criterion is easily satisfied. Typical values of the parameters are $n_e \sim 1\text{x}10^{19}$ m^{-3}, $T_e \sim 10$ eV, L ~ 0.8m, and $S_i \sim 2\text{x}10^{22}$ m^{-3}s^{-1}. $\Gamma_{\perp,\mathrm{lim}}$, shown in Figure 2c, scales linearly with the midplane pressure (which itself scales as ~ $\bar{n}_e^{\,4}$ [3,4]). The top horizontal axis shows an estimate of the

inward flux of neutrals, $\Gamma_{\perp,0}$, based on the midplane pressure. Under the assumption that the presence of the 2 poloidal limiters does not change the local radial fluxes (the local measurement is indicative of elsewhere in the outer SOL), we see that radially outward ion fluxes are balanced by the inward neutral fluxes to within a reasonable factor (~ 2). A departure from a linear relationship between fluxes to the limiter and midplane neutral pressures at the highest densities has been found for a set data taken over a wider variety of plasma currents and limiter gaps [4]. There is evidence that recycling at the outer midplane might be low compared to other poloidal locations: Pressures at the top of the vessel can be 2-10x that at the midplane. In addition, D_α measurements show that at times recycling at the inner wall can be higher than at the outer midplane. Furthermore, flux surfaces in the far SOL impact on the horizontal baffle section of the outer divertor leading to additional plasma recycling outside the lower divertor proper.

3.2 Effect of changes in core confinement

The characteristics of the far SOL appear to be relatively unaffected by the transition from L- to H-mode. In Fig. 3 we show the effects on the SOL of a transition from L- to H-mode. The far SOL is unaffected by the change in core confinement even though the line-averaged density, $\bar{n}_e$, nearly doubles. In the near SOL region the electron pressure and density as well as their gradients are larger. Utilizing these profiles and the local Ly_α emissivity [26], a local radial ion particle flux, $\Gamma_{\perp,i}$ [4,5], an effective particle diffusivity, $D_{eff} \equiv \Gamma_{\perp,i} / \nabla n_e$ (Fig. 3b), and an average radial ion velocity, $v_{\perp,i} \equiv \Gamma_{\perp,i} / n_e$(Fig. 3c), are obtained. After the transition to H-mode D_{eff} drops by about a factor of 2-3 near the separatrix as previously noted [4]. A similar drop is seen in $v_\perp$. The characteristics of radial transport in the far SOL are essentially unchanged. We note that the above estimates of velocity are lower than that found through analysis of He ion transport in the SOL of C-Mod [27] as well as the analysis of fluctuation measurements using probes [28] and D_α emission [29].

The correlation between plasma density, flux and neutral pressure at the limiter extends to H-mode plasmas. In Fig. 4 we provide, for both L-mode and H-mode plasmas, the scaling of density (Fig. 4a) and radial ion flux at the limiter radius (Fig. 4b) as well as the midplane pressure (Fig. 4c) vs. the core line-averaged density. All measures scale similarly. The L- and H-mode data points are often from the same discharge, before and after the transition. The L-H transition has the effect of an approximately horizontal translation on the graph. In other words, the measured quantity (e.g. $\Gamma_{\perp,i}$, $n_{e,lim}$) stays approximately constant while the core $\bar{n}_e$ rises during H-mode. Thus, like Figure 3, the change from L- to H-mode leaves the radial ion fluxes and resultant main chamber recycling the same. On the other hand the lack of variation of the midplane pressure from L- to H-mode might also be consistent with neutral leakage affecting the

midplane pressure: Divertor pressures (and the accompanying leakage) also do not change significantly in the transition.

4. Main chamber neutrals due to divertor neutral leakage

At issue is the level of neutral leakage out of the divertor, and whether such neutrals reach the midplane and the pressure measurement gauge. We do not directly measure the flow, rather we measure pressures and try to infer the flow magnitude relative to main chamber recycling.

4.1 General observations: lower x-point discharges

The strongest argument that neutrals are leaking out of the divertor and directly reaching the midplane measurement gauge is the correlation between the pressures measured in the divertor and at the midplane [30]. In Figure 5 we present the scaling of midplane pressure against the pressure measured at three divertor locations described in Section 2 (see Figures 1a-b): a) the lower divertor at a closed port (Fig. 5a); b) the lower divertor at an open port (Fig. 5b); and c) the upper open divertor (Fig. 5c). The data are from lower single-null discharges where the gaps and plasma current (0.8 MA) were held constant. Attached and detached divertor discharges are included. Both the lower open port divertor and upper divertor pressures correlate linearly with the midplane pressure, the scalings of the two pressures roughly a factor of 9 apart. The correlation is poorer for the lower divertor (closed port) pressure. Neutrals leak out of the lower divertor mainly through the five diagnostic openings in the outer divertor, one such location monitored by the 'open port' gauge. Thus that gauge should be proportional to the leakage flux. The neutrals that collect below closed divertor sections must travel toroidally to reach the diagnostic openings in the outer divertor before escaping the divertor towards the midplane.

The linear scaling between the lower divertor (open port) pressure (P_{LD}), upper divertor pressure (P_{UD}) and the midplane pressure ($P_{0,Mid}$) is consistent with a simple model which balances the number of neutrals entering the core plasma per unit time ($\Gamma_{\perp,0}$) across the separatrix at the outer edge (area, A_{Plasma}) with the neutral flux through lower and upper divertor leakage areas, $A_{L,Leak}$ and $A_{U,Leak}$ [30]:

$$\Gamma_{\perp,0} \equiv \beta P_{0,Mid} A_{Plasma} \approx f \cdot \beta \cdot (P_{LD} A_{L,Leak} + P_{UD} A_{U,Leak}) + \Gamma_{\perp,i} \cdot A_{Plasma} \qquad (3)$$

A term to allow for main chamber recycling has been added. We have assumed some effective transmission factor $f < 1$, for neutrals to directly stream from the divertor to the midplane. The conversion factor, β, is from the proportionality between pressure and flux. Implicit in Eq. 3 is the assumption that the measured midplane pressure is representative of a toroidal and poloidal

average of neutral pressures over the area A_{Plasma}. β drops out when Eq. 3 is converted to pressures:

$$P_{0,Mid} \approx f(P_{UD}R_{UA} + P_{LD}R_{LA}) + P_{MCR} \tag{4}$$

The contribution of main chamber recycling at outer wall surfaces is denoted by P_{MCR}. The ratio of $A_{L,Leak}$ to A_{Plasma}, R_{LA} =.0136, and $R_{UA} \sim 8xR_{LA}$.

We can use this equation as a framework for discussion of the data of Fig. 5. For such lower single-null discharges the upper divertor is just part of the main chamber. The pressures there, higher than the midplane, are due to main chamber recycling, either at the inner wall or at the top of the chamber. Since $P_{LD}R_{LA} \sim P_{UD}R_{UA}$ then the contribution to the midplane pressure due to main chamber recycling at the top of the chamber is already similar to leakage from the lower divertor. Allowing main chamber recycling at the outer wall (P_{MCR}) will reduce the relative contribution of lower divertor leakage still further.

Where are the ions coming from that produce such a large source of neutrals in the upper divertor for lower x-point discharges? If it is direct ion fluxes to the top of the vessel, then cross-field transport must be populating field lines on flux surfaces beyond the second separatrix and limiter (The upper x-point is outside the vessel for most of these data points).

Using a plausible upper limit for f (0.5) we can estimate P_{MCR}. Substituting in the scaling relationships of Fig. 5bc between P_{UD}, P_{LD} and $P_{0,Mid}$ we find $P_{MCR} \sim 0.67xP_{0,Mid}$. Inclusion of the upper chamber contribution to the midplane pressure in P_{MCR} implies that main chamber recycling contributes 80% of the midplane pressure. This simple analysis relies on the assumption of a value for f. It is also clear that the various pressures are tightly coupled (e.g. pressures on $\bar{n}_e$), making it difficult to separate out dependencies. In the remainder of this paper we will present the results of experiments where f is not assumed and one pressure is varied independent of core $\bar{n}_e$.

To give the reader some appreciation of the fluxes being discussed, we review the throughputs of such leaks. We assume that the amount of leakage is predicted by simple free molecular flow through an aperture. Given the area of the lower divertor openings, the conductance (~ 20 m^3/sec) and driving pressure lead to leakage fluxes in the range 0.5-2 $x10^{22}$ particle/sec for typical lower open divertor conditions (5-20 mTorr). This neutral leak rate is of similar magnitude as the radial ion fluxes shown in Fig. 2c and the integrated ion flux to the lower outer divertor plate. The torus gas puff rate used to maintain the plasma density is about a factor of 20 smaller!

4.2 Effect of changes in up-down divertor balance

Because the divertor and midplane pressures are so strongly correlated with each other and with the core plasma line-averaged density we have attempted to find ways of varying the divertor pressure, and thus the source of neutral leakage, independent of $\bar{n}_e$. Our primary method for divertor pressure control is to vary the magnetic equilibrium from single-null x-point at the lower divertor to double-null (symmetric up-down x-points). Using SSEP as a measure of divertor dominance, Fig. 6 shows the upper divertor, midplane and lower divertor (closed and open ports) pressures vs. SSEP. When SSEP is a large negative value the lower divertor pressures are much higher than that at the upper divertor. At the other extreme, when the equilibrium is double-null (SSEP=0), the two divertor pressures are closer. Ignoring outlier points, the midplane pressure may be considered to increase slightly as SSEP approaches 0.

We can use a simpler version of Eq. 3 for analysis of this data:

$$\Delta P_{0,Mid} = \alpha \cdot (\Delta P_{LD} + 8 \cdot \Delta P_{UD}) + \Delta P_{MCR} \tag{4}$$

where $\alpha = f \bullet R_{LA}$ and $R_{UA}/R_{LA} \sim 8$. Since the core conditions were held approximately constant, we assume the same for P_{MCR} and the last term drops out. We thus derive a value of α (and ***f***) that fits the data, and solve for P_{MCR} using Eq. 3. The curves in Fig. 6 show the result of fitting the pressure data from the divertors and the model prediction of the midplane pressure with the derived value of α = .002 (***f*** ~ 12.5%). The contribution to the midplane pressure are $\boldsymbol{P_{MCR}}$ /$\boldsymbol{P_{0,Mid}}$ ~ 0.9 and $\boldsymbol{P_{L,Leak}}$ /$\boldsymbol{P_{0,Mid}}$ ~ 0.1.

We note that this estimation of $P_{MCR}/P_{0,Mid}$, and those following, are not dependent on knowing the values of ***f,*** R_{LA} and R_{UA}. They are absorbed into one fit parameter, α, which is then used to determine $P_{MCR} = P_{0,Mid} - \alpha \cdot (P_{LD} + 8 \cdot P_{UD})$.

4.3 Effect of upper x-point discharge

Based on the results shown in Figure 6 discharges were programmed to take SSEP beyond 0 to achieve upper single-null dominant equilibria. Two discharges are shown in Figure 7, one with SSEP (Fig. 7a) varied from –15 mm to + 8 mm, the other with little SSEP variation for reference. The plasma, formed limited on the inner wall, becomes diverted at ~ 0.25 seconds. The density reaches an equilibrium value of 0.95 x 10^{20} m^{-3} at 0.5 seconds. As the magnetic equilibrium becomes double-null (SSEP=0), the upper and lower divertor (closed) pressures reach similar values as seen in Figure 6. The outer wall pressures (Fig. 7c-e) at the three poloidal locations appear to equalize at a lower value. At the largest values of SSEP (and thus the upper divertor pressure) there are signs of leakage from that divertor affecting the outer wall (upper) pressure and that at the midplane. As for the data of Fig. 6, changes in lower divertor leakage

have little effect on the midplane pressure. More telling is that the leakage from the upper divertor (~1.25 sec) reaches values ~ 8x that from the lower divertor (~.65 sec), and yet the relative increase in the midplane pressure is only in the range 1.7-2.

When we apply the neutral flux balance model to the data of Figure 7 we find the same values of α (~ .002) & $\boldsymbol{f}$ (~12 %) give a good fit to the time variation in outer wall (midplane) pressure due to neutral leakage out of the divertors. The lower divertor contribution to the midplane pressure is again small (≤ 10% of $\boldsymbol{P_{MCR}}$), even for the highest lower divertor pressures shown in Figure 7. The upper divertor leakage contribution rises to ~ 0.7-1.0x $\boldsymbol{P_{MCR}}$ as the upper divertor pressure rises.

4.4 Effect of changes in inner limiter gap

Supporting evidence for the dominance of main chamber recycling comes from another experiment where the plasma was limited on the inner wall. Fig. 8 shows a comparison of limited vs. standard divertor operation for two cases - outer gap of 15 mm and 25 mm. The height of the plasma was unchanged leading to slight variations in elongation due to the varying width of the plasma equilibrium. The lower (closed) divertor pressure (Fig. 8a) is reduced by reduced power flow into the divertor as the plasma becomes limited. But the midplane pressure (Fig. 8b) is relatively unaffected. The lower (open) port pressure measurement was not working for this run, but in general, its pressure is 2-3 x lower (Fig. 5 includes similar $\bar{n}_e$ discharges where the ratio was ~ 2.5) than the closed port for such attached discharges. Since the upper chamber pressures are extremely low (0.1 mTorr) and do not change for these experiments then it is unlikely that the large neutral source created at the inner wall is affecting the outer midplane pressures. Thus the large drop in lower divertor pressure should lead to a large drop in midplane pressure if leakage dominates the midplane pressure. This clearly is not the case. The analysis using Eq. 4 yields α =.005-.0010, f =.33-.72 and the fraction of $P_{0,Mid}$ due to main chamber recycling, $P_{MCR}/P_{0,Mid}$, is ~ 74-87%.

We have also limited the plasma on the outer poloidal limiters while keeping the inner gap constant. The midplane pressure only rises slightly, even though the local limiter fluxes are estimated to increase by a factor of 8. The plasma profiles in the shadow of these limiters measured near the divertor entrance do not change much, indicating the general SOL away from the limiter is relatively unaffected. The divertor pressure and plasma characteristics change. We cannot account for where the neutrals, created at the limiter surfaces, go. These data are not consistent with any particular explanation of what dominates the midplane pressure. Further analysis and experiments are required.

4.5 Effect of toroidal variation in leakage

The above experiments indicate that a significant fraction of neutrals leaking from through the divertor structure do not reach the midplane. We have executed a series of experiments aimed at estimating the transmission fraction of neutrals by an independent method. Figure 9 shows the result of one discharge where the divertor bypass valves from three toroidally-adjacent bypass locations (at –18°, 18°, 54°, Fig. 1b) were opened and closed with period 200 ms during plasma discharges. The locations of the various pressure gauges relative to the bypass valves can be found in Fig. 1. The plasma current is held constant and $\bar{n}_e$ (Fig. 9a) is increasing. Helium was utilized as the fuel gas for these experiments to eliminate the uncertainty of the role of the wall as a reservoir for neutrals. During the period that the bypass valves are opening or closing (~ 20 ms, shaded regions, Fig. 9b), there is a prompt effect on the outer wall (lower) Penning gauge (Fig. 9e). We attribute this to neutrals directly reaching the gauge from the nearby bypass valves. The midplane gauges (9d), the divertor gauge (9f) and $\bar{n}_e$ show similar, slower, changes. The small change in the outer wall (upper) gauge (9c) potentially exhibits some of the same prompt effect as the outer wall (lower) gauge but the effect is very small.

We also varied the location of the three adjacent valves from near to the Penning gauges to far from them. Figure 10a-b shows the effect on $\bar{n}_e$ and the outer wall (lower) gauge for one valve cycle, including the case from Figure 9 (shown as a solid line) as well as a case where the closest of the three valves was 72 degrees away from the outer wall gauge (dashed line). When the bypass valves are farther away from the gauge, the prompt effect on the outer wall (lower) gauge disappears and its change in pressure is smaller relative to the increase in density. The result of varying the toroidal locations of valves to still more locations is summarized in Figures 10c-d. The change in pressure measured at the outer wall lower (10c) and midplane (10d) gauges are plotted against the change in density caused by the release of gas. The data are grouped by cases where the valves are located just by the gauge (circles) and for valves located 72-108 degrees away (triangles). These results indicate that only the region of the outer wall poloidally and toroidally near the outer divertor valve is affected directly by neutral leakage. In addition, ~50% of the pressure rise on the outer wall gauge near the bypass valves is due to a toroidally uniform rise (Fig. 10c). We find ~ 20 degree e-folding distance toroidally (~20 cm) for the prompt effect. The poloidal decay length is difficult to estimate but based on the change in outer wall (upper, Fig. 9c) gauge relative to that of the outer wall (lower, Fig. 9e), it appears to be of order 40-50 cm. Thus it would appear that most of the neutrals leaking from the divertor are converted to ions, travel around the torus and recycle in the main chamber near other gauges. This would explain the toroidally uniform pressure rise as well as the slow time behavior correlation between the gauges and the core $\bar{n}_e$.

5. Discussion

5.1 Main chamber neutrals due to cross-field transport

There is certainly a large quantity of evidence, both in this paper and in previous work, that the magnitude and scaling of cross-field ion transport in C-Mod can explain measured midplane pressures. In this paper we further explore the effect of the transition from L- to H-mode. The effects of the energy confinement change are limited to the core and the near SOL in these ohmic H-mode plasmas. Since the cross-field ion flux in the SOL does not significantly change, the core density rises to be consistent with reduced cross-field transport near the separatrix.

Let us explore what it means for cross-field transport to compete effectively with parallel transport. One way to quantify the 'strength' of radial, compared to parallel, transport is to determine a $\mathrm{v}_{\perp,\min}$ needed for the ion flux crossing a given flux surface, $\Gamma_{\perp,i}$, to be equal to the integral of the parallel ion flux flowing to the divertor from that flux surface on outwards:

$$\Gamma_{\perp,i} = n\mathrm{v}_{\perp,\min} 2\pi R L_{pol} \sim nMc_s \frac{B_{pol}}{B_{Tor}} 2\pi R \lambda_{\perp}, \qquad \mathrm{v}_{\perp,\min} \sim Mc_s \lambda_{\perp} / L \tag{8}$$

We have approximated the integral of parallel fluxes by $2\pi R\lambda_{\perp}$. For M = 1, then $\mathrm{v}_{\perp,\min}$ (Fig. 3d) is similar in magnitude $\mathrm{v}_{\perp,i}$ (Fig. 3c) obtained from the continuity analysis. We see that the two profiles are very similar in magnitude and shape. If, as experimental data from the vertical scanning probe at the entrance of the divertor has shown [4], that flow is more in the range of M=0.1, then radial fluxes are more likely to be dominant. The relative magnitude of perpendicular and parallel velocities has potential consequences for the SOL and main chamber recycling. For example, the effect of inserting of a limiter into the SOL would be reduced as perpendicular transport becomes more dominant, essentially 'filling-in' around obstacles. This 'filling-in' effect would be further enhanced by ionization in the limiter shadow.

We believe that the strong radial transport in the far SOL is convective in nature. Figure 2a-b indicates that in regions lacking gradients in density (far SOL) or T_e (shadow of a limiter) power is being transported across the magnetic field, enough to sustain the plasma there against parallel conduction as well as the cost of ionizing neutrals. That is evidence of convected power.

An indirect effect of main chamber recycling is that impurity sources are created on surfaces close to the plasma core. Such impurity sources have a higher probability of reaching the plasma core than impurities originating in the divertor [31-34]. Better determination of the locations of main chamber recycling and impurity sources are needed.

5.2 Main chamber neutrals due to neutral leakage

A simple model, embodied in Eq. 4, was applied to a wide variety of data. Values of the fraction of the midplane pressure supplied by main chamber recycling range from 70 – 90%. Based on our limited data set we cannot determine if the variation in relative contributions of leakage and main chamber recycling to the midplane pressure is significantly dependent on plasma conditions.

The divertor bypass valve experiments approach the neutral leakage from another point of view. The results from the analysis of Figures 9 and 10 indicate that the transmission of neutrals directly to the midplane poloidally is in the range 30-50%. The flux balance analysis (Eq. 4) of the data in Figures 6-8 yields similar values.

There are aspects of the measurements and model that need further investigation. For example, our experiments indicate fairly short toroidal and poloidal e-folding lengths for the direct effect of released neutrals (recycling or divertor leakage). The large number of structures in the outer SOL and the localized nature of divertor leakage openings would indicate that measuring the pressure at one or two toroidal locations is probably not adequate for fully characterizing the 'outer midplane' pressure.

Another concern raised by the measurements and analysis contained herein is the possibility that utilizing a free-molecular flow model to estimate divertor leakage may not be appropriate. There are several aspects to this: First, divertor pressures are measured in a vertical port. Are such pressures true measurements of the pressure (and thus fluxes) at the leakage aperture? Previous comparisons of measurements at these two locations indicated little difference [35]. Secondly, we know that the SOL plasma extends far into the shadow of limiters. This leads to the existence of plasma directly above the leakage apertures in C-Mod. Such plasma could enhance the albedo of the plasma through charge-exchange and neutral-neutral collisions, thus reducing the effective conductance out of the aperture. This type of effect has been utilized to explain the lack of private flux zone pressure loss through the divertor plasmas during divertor detachment [35]. Thirdly, the free-molecular conductance calculation of leakage fluxes assumes zero pressure outside the aperture. This is unlikely to be true.

There has been much success in the use of 2-D SOL/divertor transport codes to model the divertor plasma and its interaction with the divertor surfaces. Such codes are essential for determining the efficacy of the axisymmetric poloidal divertor with respect to alternative (e.g. ergodic divertor, limiter, or even stellarator) heat and particle flux handling configurations. At present the SOL/divertor modelling codes do not normally include interactions with objects in the far SOL, perhaps beyond even the second separatrix. The results herein thus raise concerns about the 2-D code predictions with respect to the SOL plasma and wall interactions.

It is not clear how applicable these results are to other variations in divertor geometry. Our primary concern is that the location of the divertor leakage pathway may be very important in determining its influence on midplane pressures. For example, the closer the leakage outlet is to the midplane and the farther it is from the SOL plasma, the larger effect it may have.

6. Summary

The results of a series of experiments aimed at better quantifying the relative contribution of divertor leakage and radial ion transport on neutral pressures surrounding the core are described. We find that cross-field transport competes with, or dominates, parallel transport in such a way that plasma exists far out in the SOL shadow, thus leading to recycling. Changing the core transport from L- to H-mode leads to little or no effect on the far SOL indicating that the flux to the walls has not changed, just the gradients at the separatrix and the density in the core.

The recycling in the main chamber due to cross-field transport appears to be an important source for neutrals for lower divertor operation. Estimates of the contribution of lower divertor leakage to the midplane pressure range from 10-30%. At this time we do not know whether the relative contributions to the main chamber pressure by main chamber recycling and lower divertor leakage vary with operating conditions. The leakage out of the upper divertor is much higher than from the lower divertor. Even so, we find its contribution to the midplane pressure to be similar to that of main chamber recycling.

Divertor bypass valve experiments show that neutrals flowing out of the outer divertor are attenuated as they travel towards the midplane and around the torus. The observed toroidal and poloidal e-folding lengths for the escaping neutrals are ~ 20 and 50 cm respectively. Such attenuation of neutrals is consistent with the estimates of the effect of neutral leakage on the midplane pressure. The importance of neutral leakage might be significantly altered if the location where neutrals escape into the main chamber were located farther from the plasma, allowing easier passage around the plasma.

Acknowledgements – The authors would like to thank C. Boswell and S. Wolfe for invaluable assistance in the second separatrix scan studies. We also thank J. Goetz, P. Stangeby, J. Terry and D. Whyte for many stimulating discussions. This work supported by the U.S. Department of Energy under Grant No. DE-FC02-99ER54512.

References

[1] Umansky M. V., Krasheninnikov S. I., LaBombard B., and Terry J. L. 1998 *Physics of Plasmas* **5** 3373

[2] Umansky M. V., Krasheninnikov S. I., and LaBombard B. 1999 *Physics of Plasmas* **6** 2791

[3] Labombard B., Lipschultz B., Goetz J. *et al*, "Cross-field transport in the SOL: Its relationship to main chamber and divertor neutral control in Alcator C-Mod," in *Plasma Physics and Controlled Fusion Research* (IAEA, Vienna (2001), Sorrento, 2000).

[4] LaBombard B., Umansky M. V., Boivin R. L. *et al* 2000 *Nuclear Fusion* **40** 2041

[5] LaBombard B., Boivin R. L., Greenwald M. *et al* 2001 *Physics of Plasmas* **8** 2107

[6] Bosch H. S., Neuhauser J., Schneider R. *et al* 1995 *Journal of Nuclear Materials* **220-220** 558

[7] Pitcher C. S., Boswell C. J., Goetz J. A., LaBombard B., Lipschultz B., Rice J. E., and Terry J. L. 2000 *Physics of Plasmas* **7** 1894

[8] Loarte A. 2001 *Plasma Physics & Controlled Fusion* **43**

[9] Horton L. D., Vlases G. C., Andrew P. *et al* 1999 *Nuclear Fusion* **39** 1

[10] Kawashima H., Sengoku S., Ogawa T., Ogawa H., Uehara K., Miura Y., and Kimura H. 1999 *Nuclear Fusion* **39** 1679

[11] Allen S. L., Brooks N. H., Bastasz R. *et al* 1999 *Nuclear Fusion* **39** 2015

[12] LaBombard B., Goetz J. A., Hutchinson I. *et al* 1997 *Journal of Nuclear Materials* **241-243** 149

[13] Bosch H. S., Ullrich W., Bard A., Coster D., Haas G., Kallenbach A., Neuhauser J., and Schneider R. 1999 *Journal of Nuclear Materials* **266-269** 462

[14] Schneider R., Bosch H. S., Coster D. *et al* 1999 *Journal of Nuclear Materials* **266-269** 175

[15] Monk R. D. 1999 *Nuclear Fusion* **39** 1751

[16] Pitcher C. S., LaBombard B., Danforth R., Pina W., Silveira M., and Parkin B. 2001 *Review of Scientific Instruments* **72** 1

[17] Lao L. L., St. John H. , Stambaugh R. D., Kellman A.G., Pfeiffer W., and 1611 Nucl. Fusion 25 (1985) 1985 *Nuclear Fusion* **25** 1611

[18] Ulrickson M. and Post D. E. 1983 *Journal of Vacuum Science & Technology A-Vacuum Surfaces & Films* **1** 907

[19] McCormick K., Fiedler S., Kyriakakis G., Neuhauser J., Reiter D., Schneider R., Schweinzer J., and N. Tsois N., "Particle and Energy Transport in the ASDEX Scrape-Off Layer," in *Controlled Fusion and Plasma Physics* (European Physical Society, Geneva (1993), Lissabon, 1993), Vol. 2, pp. 597.

[20] Asakura N., Koide Y., Itami K., Hosogane N., Shimizu K., Tsuji-Iio S., Sakurai S., and Sakasai A. 1997 *Journal of Nuclear Materials* **241-243** 559

[21] Shimizu K., Itami K., Kubo H., Asakura N., and Shimada M. 1992 *Journal of Nuclear Materials* **196-198** 476

[22] Owen L., Carreras B., Mioduszewski P., Boivin R. L., Hubbard A. E., LaBombard B., Pitcher C. S., and Terry J. L. 1998 *Bull. Amer. Phys. Soc.* **43** 1823
[23] Stangeby P. C. 1984 *Journal of Nuclear Materials* **121** 55
[24] Staib P. 1980 *Journal of Nuclear Materials* **93 & 94** 351
[25] Staudenmaier G., Staib P., and Poschenrieder W. 1980 *Journal of Nuclear Materials* **93 & 94** 121
[26] Boivin R. L., Goetz J. A., Hubbard A. E. *et al* 2000 *Physics of Plasmas* **7** 1919
[27] Nachtrieb R. and LaBombard B. 2000 *Physics of Plasmas* **7** 4573
[28] Carreras B., Lynch V.E., and LaBombard B. 2001 *Physics of Plasmas* **8** 3702
[29] Terry J. L., Maqueda R., Pitcher C. S., Zweben S. J., LaBombard B., Marmar E. S., Pigarov AYu, and Wurden G. 2001 *Journal of Nuclear Materials* **290** 757
[30] Pitcher C. S., Erents S.K., Fundamenski W. *et al* 2001 *Proc. of the 28th Eur. Physical Society Conf. on Controlled Fusion and Plasma Physics* (Madeira, Portugal, 18-22 June 2001) NA
[31] Janeschitz G., Konig R., Lauro-Taroni L. *et al* 1992 *Journal of Nuclear Materials* **196-198** 380
[32] Matthews G.F., Stangeby P.C., Elder J.D. *et al* 1992 *Journal of Nuclear Materials* **196-198** 374
[33] McCracken G. M., Lipschultz B., Labombard B. *et al* 1997 *Physics of Plasmas* **4** 1681
[34] Lipschultz B., Pappas D. A., LaBombard B., Rice J. E., Smith D., and Wukitch S. J. 2001 *Nuclear Fusion* **41** 585
[35] Niemczewski A., Hutchinson I. H., LaBombard B., Lipschultz B., and McCracken G. M. 1997 *Nuclear Fusion* **37** 151

Figure captions:

Figure 1: Poloidal (a) and toroidal (b) cross-sections of Alcator C-Mod the lower closed divertor and open upper divertor. Baratron capacitance manometer pressure gauges are located in the vertical ports at locations 1,9 and 10. A shielded Bayard-Alpert gauge is at location 5 in a horizontal port. Penning gauges are attached the wall of the vessel at locations 3 & 6. Scanning probes are inserted horizontally (4) and vertically (7). Divertor bypass valves are located at 10 points toroidally (8). Two thin plates/gussets (#2, shown as dotted lines in 1a, of ~ 1.25 cm toroidal extent, are located on either side of each of 10 vertical ports with protection tiles on the edge facing the plasma.

Figure 2: SOL parameters and the effect of increasing $\bar{n}_e$. a) n_e profiles; b) T_e profiles; c) scaling of the inferred radial ion flux density at the limiter radius, $\Gamma_{\perp,\mathrm{lim}}$, vs. midplane pressure (lower axis) and equivalent radial influx of neutrals (upper axis). Shaded regions in a) and b) correspond to the range of limiter radii occurring over these shots.

Figure 3: Effect of transition from L- (open circles) to H-mode (closed circles) on the SOL. The H-mode density data is from a time ~ 140 msec after the transition when the core density is close to its H-mode level of 2.6×10^{20} m^{-3} (from 1.6×10^{20} m^{-3} in L-mode). a) n_e profile; b) D_{eff} profile; c) $v_\perp$ profile; and d) $v_{\perp,\mathrm{min}} \sim Mc_s\lambda_\perp / L$. The location of the limiter surface is given by the vertical shaded region.

Figure 4: Scaling of the density at the limiter radius, $n_{e,\mathrm{lim}}$ (a), $\Gamma_{\perp,\mathrm{lim}}$ (b), and midplane pressure (c, location 5 in Figure 1) vs. $\bar{n}_e$. L-mode (open circles) and H-mode (closed circles) are shown. The H-mode discharges have the same far SOL parameters as the L-mode discharges from which they arose.

Figure 5: Scaling of outer wall (midplane) pressure vs. various divertor pressures during lower x-point, 800 kA, L-mode discharges. a) Lower divertor (closed); b) lower divertor (open port); and c) open upper divertor. Detached plasmas are shown as filled symbols. Fits to the various data sets are shown as lines.

Figure 6: Utilization of the first to second separatrix gap at the outer midplane (SSEP) to change the divertor pressures and the resultant effect on the outer wall (midplane) pressure. SSEP is varied from discharge to discharge from lower single-null to double-null (SSEP= -15 to 0 mm).

L- and H-mode cases are included. The lines shown are the fits to the divertor pressures, used in Eq. 6, as well as the resultant prediction of the midplane pressure.

Figure 7: The effect of an SSEP scan in one shot from single null at the lower divertor (SSEP < 0) to single-null at the upper divertor (SSEP > 0) is given by the solid line. A reference case with the standard single-null at the lower divertor is also shown (long dashed line). The vertical short-dashed line indicates when the equilibrium becomes double-null.

Figure 8: Effect on the divertor and outer wall (midplane) pressures of limiting the plasma on the inner wall.

Figure 9: Three divertor bypass valves (toroidal locations –18°, +18°, +54°) are opened and closed with ~ 200 ms full period. The period when the bypass valves are opened or closed is shaded and marked in b). The relative toroidal locations of the valves and gauges are given in Fig. 1b).

Figure 10: Summary of the results from discharges where the toroidal location of the 3 bypass valves is varied. The data are divided into two cases – bypass valves opened near the outer wall (lower) gauge (solid lines and circles) and far from that gauge (dashed lines and triangles). a) change in $\bar{n}_e$ vs. time; b) change in outer wall (lower) pressure vs. time; c) change in outer wall (lower) pressure vs. change in $\bar{n}_e$; and d) change in outer wall (midplane) pressure vs. change in $\bar{n}_e$.

Figure 1

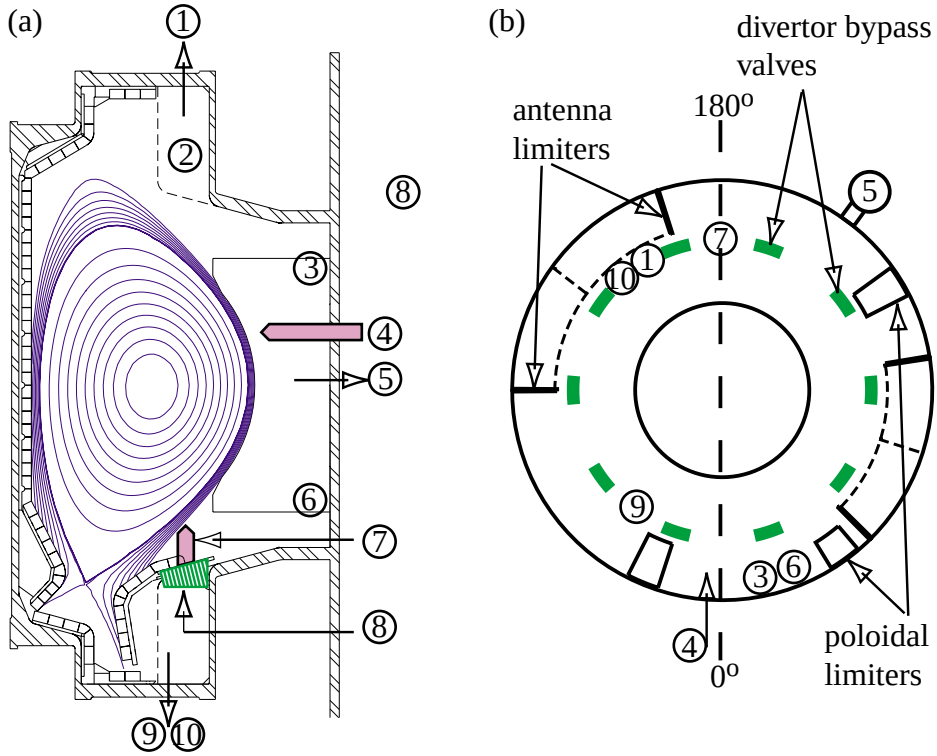

Figure 2

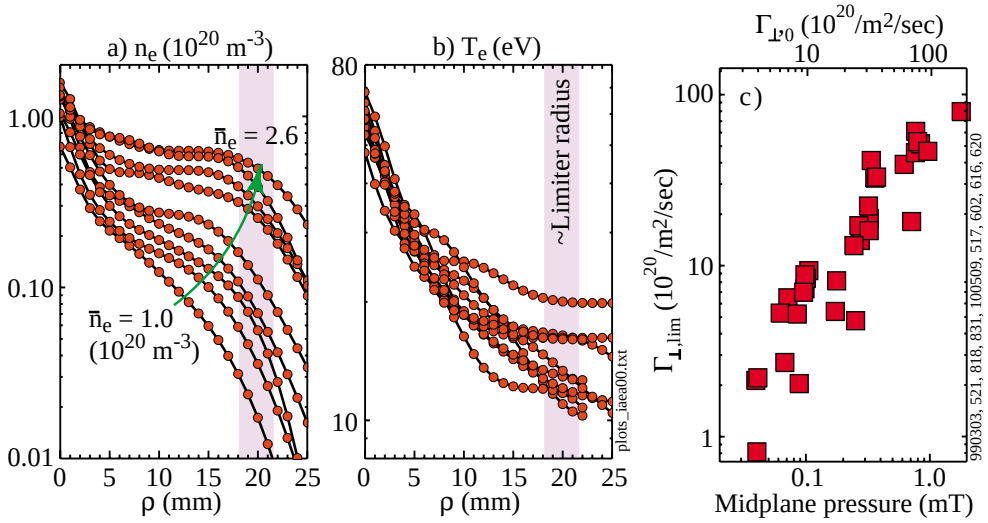

Figure 3

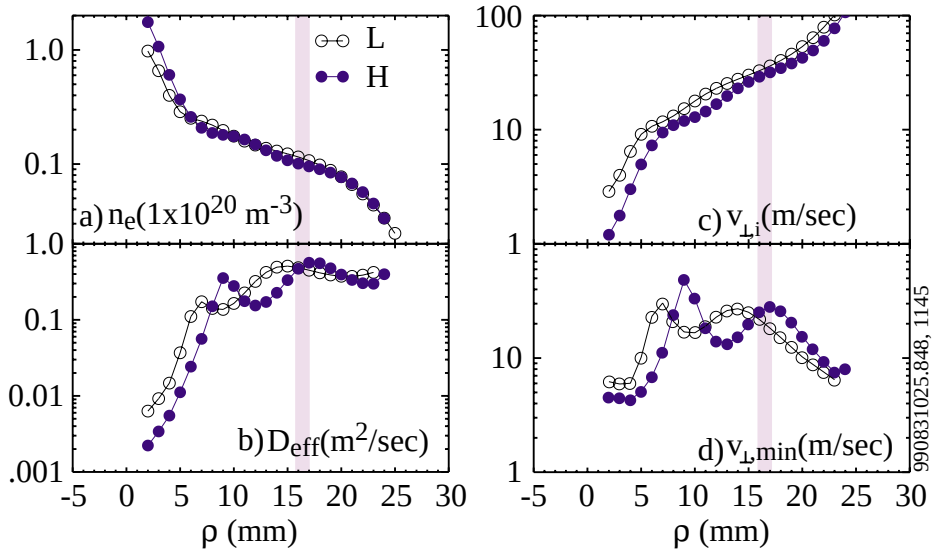

Figure 4

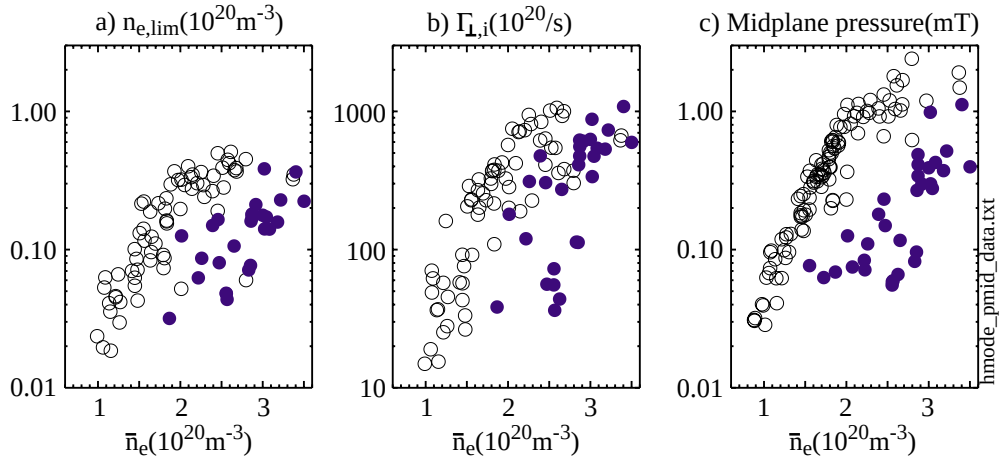

Figure 5

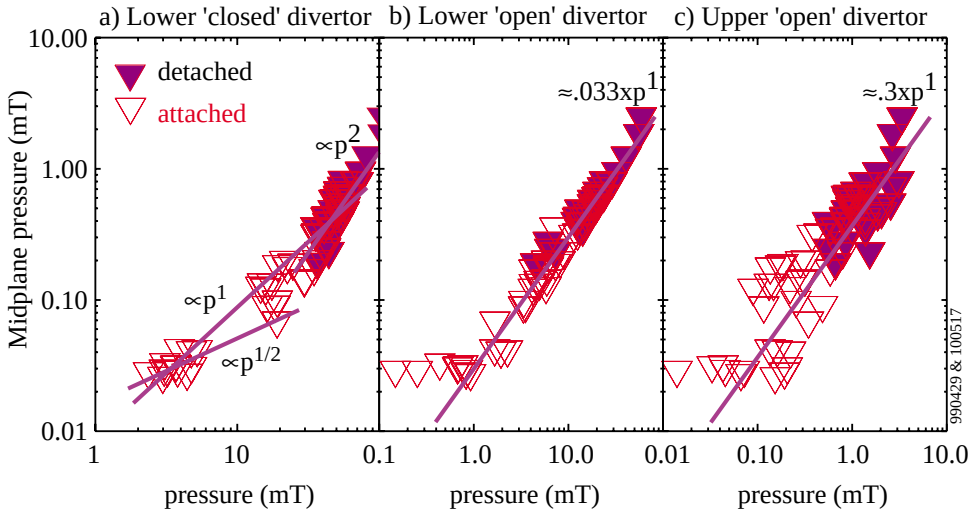

Figure 6

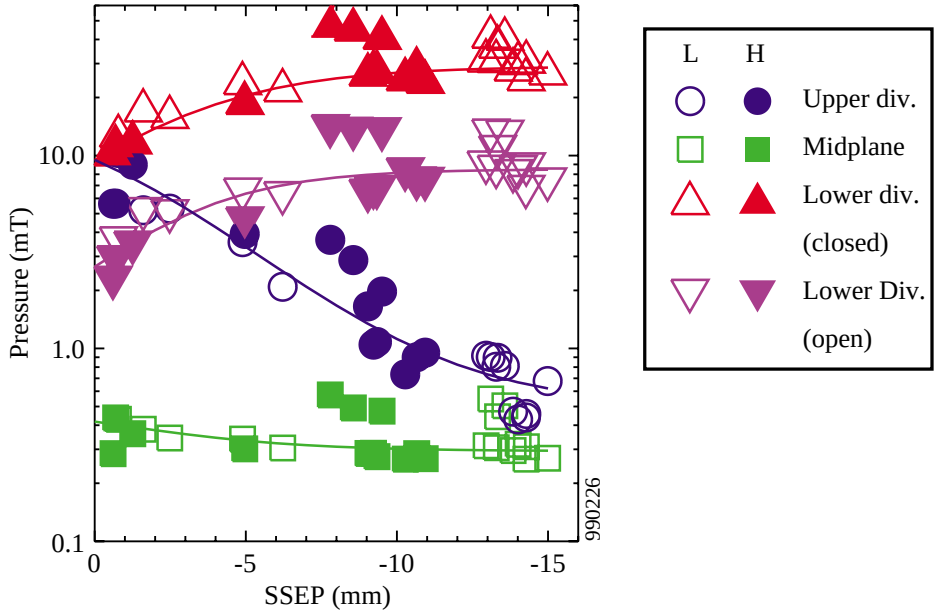

Figure 7

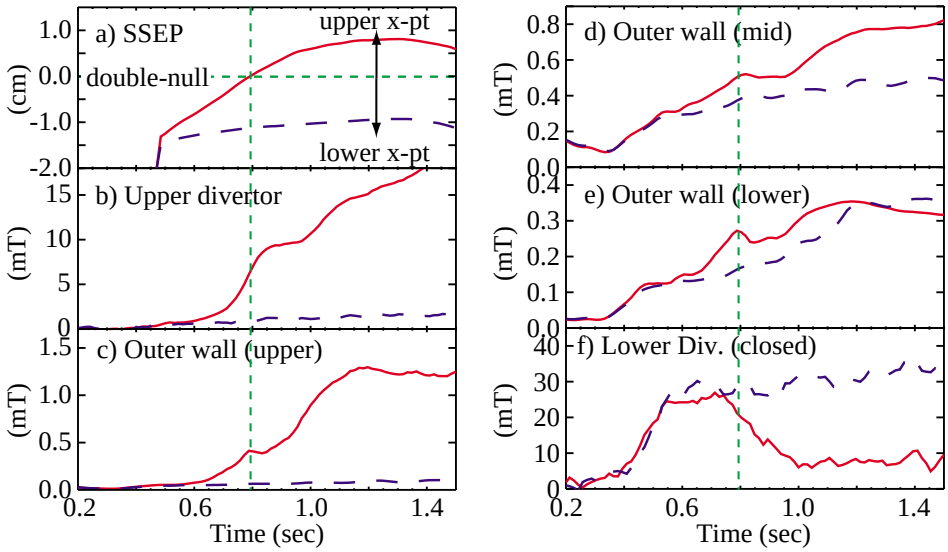

Figure 8

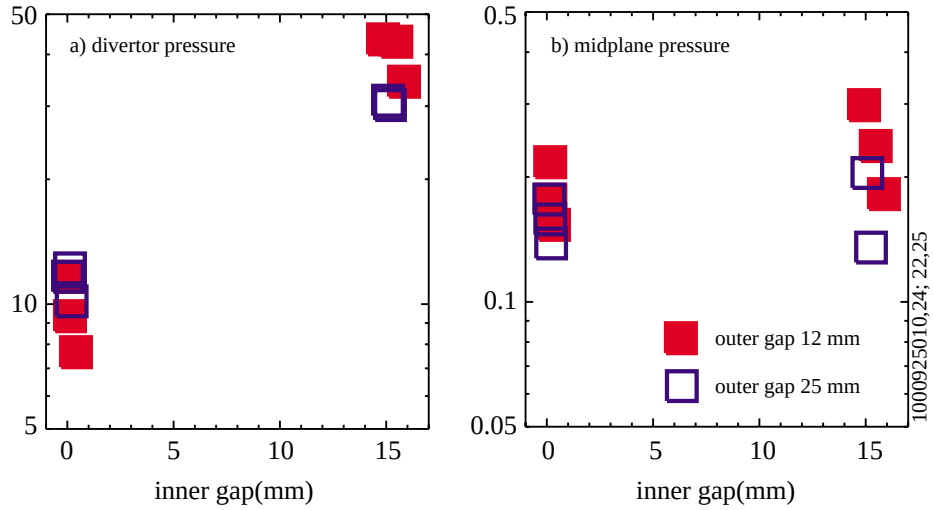

Figure 9

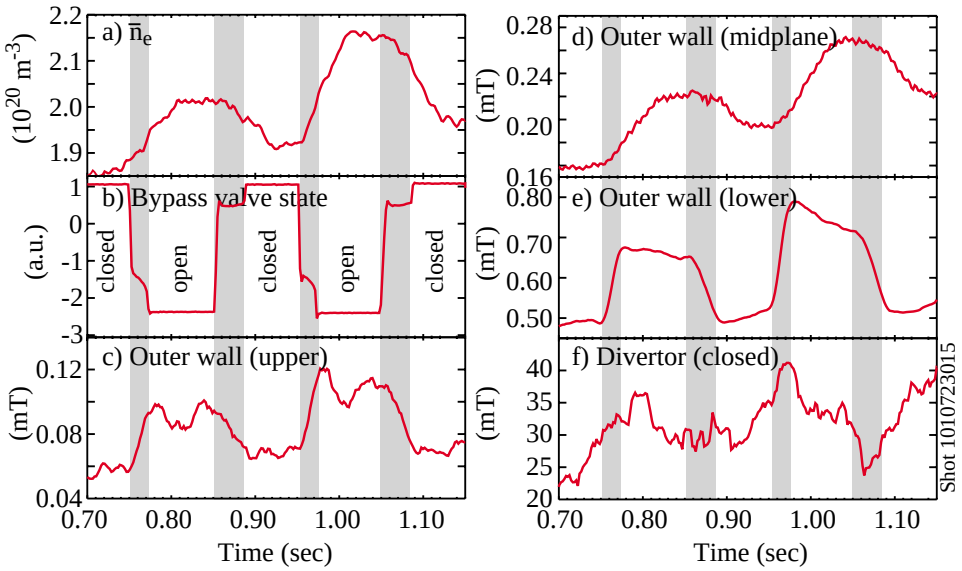
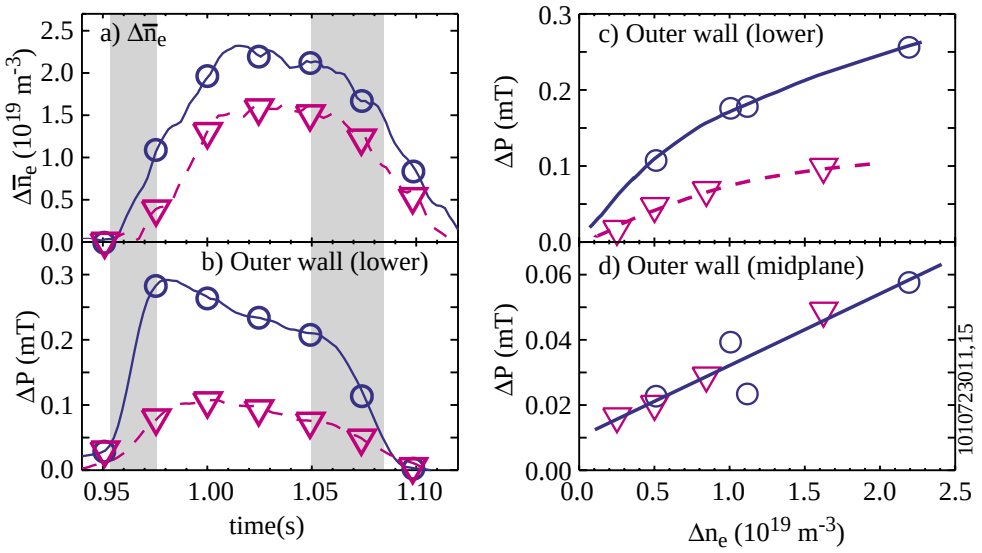
Figure 10